ISSN 1063-7729, Astronomy Reports, 2009, Vol. 53, No. 6, pp. 519–527. © Pleiades Publishing, Ltd., 2009.
Original Russian Text © V.I. Slysh, S.V. Kalenskii, 2009, published in Astronomicheskiĭ Zhurnal, 2009, Vol. 86, No. 6, pp. 564–573.

Structure of the Class I Methanol Masers OMC-2 and NGC 2264

V. I. Slysh† and S. V. Kalenskii

Astrospace Center, Lebedev Institute of Physics, Russian Academy of Sciences, Profsoyuznaya ul. 84/32, Moscow, 117997 Russia

Received October 22, 2008; in final form, November 7, 2008

Abstract—Results of interferometric observations of the class I methanol masers OMC-2 and NGC 2264 in the $7_0-6_1A^+$ and $8_0-7_1A^+$ lines at 44 and 95 GHz, respectively, are presented. The maser spots are distributed along the arcs bent toward infrared sources, which are young stellar objects. The distributions of the maser spots at 44 and 95 GHz are virtually identical, and the fluxes from the brightest spots are similar. The measured sizes of the maser spots at 44 GHz are, on average, about 50 AU. The brightness temperature of the strongest components at 44 GHz is 1.7×10^7 K and 3.9×10^7 K for OMC-2 and NGC 2264, respectively. A simple model for the excitation of Class I methanol masers is proposed; it yields an estimate of the limiting brightness temperature of the emission. The model is based solely on the properties of the methanol molecule without invoking the physical parameters of the medium. Using it, we showed that the emission opening angles for NGC 2264 and OMC-2 do not exceed 3° and 4.5°, respectively. The depth of the masing region is about 1000 AU. The emission directivity is naturally realized in the model of of maser consisting of a thermalized core and a thin inverted envelope, probably, with an enhanced methanol abundance. The maser emission has the greatest intensity in the direction tangential to the envelope. The size of the masing envelope estimated from the measured depth and spot extens is $\sim 2 \times 10^4$ AU, or 0.15 pc. This size is close to the sizes of the dense molecular cores surrounding the young stellar objects IRS 4 in OMC-2 and IRS 1 in NGC 2264.

PACS numbers: 98.38.Er, 98.38.Dq, 95.85.Bh
DOI: 10.1134/S1063772909060043

1. INTRODUCTION

Methanol masers, along with OH and H_2O masers, are associated with star-forming regions and molecular clouds. However, in contrast to the OH, H_2O, and Class II methanol masers immediately adjacent to young stars and protostars at a distance of several thousand AU from the central object, class I methanol masers are located much farther, at a distance of up to a hundred thousand AU (fraction of a parsec) [1]. Maser spots on the maps of Class I methanol masers are probably located at the forefront of bipolar outflows from star-forming regions [2]. However, a more detailed study does not reveal an unambiguous correspondence between maser spots and bipolar outflows [3]. Moreover, there is no coincidence between the positions of individual spots and cloudlets of molecular hydrogen emission, which results from the heating by a shock wave driven by a bipolar flow. The absence of physical objects toward maser spots has led to a model of maser emission in which the masers arise in extended molecular clouds with an average optical depth in maser transitions that is small over the cloud. Due to the presence of a turbulent velocity field in the cloud, in some directions, the velocity gradients can occasionally be small, thus favoring coherent maser amplification. In an unsaturated mode, the amplification depends on the coherence length exponentially; this results in a large intensity contrast and in the formation of bright maser spots [4].

Mapping masers with a high resolution is necessary for comparison with maps of the masing region in other wavelength ranges. The highest linear resolution can be achieved for the nearest masers. OMC-2 and NGC 2264 belong to the nearest class I methanol masers. OMC-2 is one of the three large molecular clouds (OMC-1, OMC-2, and OMC-3) of the Orion Bar, which contains a great number of protostars, young stars, and molecular outflows. The source OMC-2 is at a distance of about 400 pc, near the pair of the infrared sources IRS 4N and IRS 4S [5]. Another nearby maser is associated with the open star cluster NGC 2264 at a distance of 700 pc, near the bright infrared source IRS 1 (Allen's source [6]). In this paper, we report the results of mapping these masers in two methanol lines at 44 and 95 GHz and propose a model of Class I methanol masers.

†Deceased.

Table 1. Absolute positions of methanol masers and adjacent bright infrared sources

Object	$\alpha(2000)$	$\delta(2000)$	V_{LSR}, km s^{-1}
OMC-2	$05^h35^m27.813^s$	$-05°09'42.77''$	11.25
IRS 4S*	05 35 27.5	−05 09 37.6	
NGC 2264	06 41 08.840	09 29 32.54	7.24
IRS 1**	06 41 10.17	09 29 33.7	

* Position taken from [5]
** Position taken from [6].

Table 2. Characteristics of maser spots in OMC-2 at 44 GHz

Spot	$\Delta\alpha$	$\Delta\delta$	V_{LSR}, km s^{-1}	Flux density, Jy
A	$-1.53''$	$-3.43''$	11.94	2.0
B	0.12	0.56	11.55	23.0
C	−2.25	−4.39	11.76	1.4
D	0	0	11.26	229
E	0.04	0.30	11.30	13
F	0.20	0.51	11.13	21

2. OBSERVATIONS

The methanol masers OMC-2 and NGC 2264 were mapped in two transitions, $7_0-6_1A^+$ at 44.06943 GHz on VLA NRAO in October 1998 and $8_0-7_1A^+$ at 95.16944 GHz on BIMA (consortium of the Berkeley–Illinois–Maryland Universities) in February 1998. The synthesized VLA beamwidth was about $0.15''$, and that of BIMA at 95 GHz was $0.5''$. The spectral resolution was 0.042 and 0.15 km s^{-1} at 44 and 95 GHz respectively. The VLA 44-GHz observations of the masers at 44 GHz were carried out in the reference source mode; as a reference source, we used for OMC-2 the compact calibrator VLA 05392−05433, and for NGC 2264 the calibrator VLA 06571+17136. Therefore, it was possible to measure the absolute coordinates of masers to an accuracy of the order of $0.01''$, which is much higher than the accuracy of previous measurements of the absolute positions of Class I masers in various star-forming regions [2, 7, 8]. This allows us to tie the maser spots to the maps in the infrared and submillimeter ranges. On BIMA at 95 GHz only the positions of maser spots with respect to the reference spot (the strongest one) were determined. This allowed us to eliminate the variable effect of the atmosphere, which is so important at this frequency that it makes the measurement of the absolute positions using reference sources impossible.

The results of the observations were processed using the NRAO AIPS software package developed for interferometric measurements. The amplitude and phase calibration of individual VLA antennas was implemented using reference calibration sources. Owing to this calibration, the array of antennas was phased, and masers were mapped in each spectral channel where an appreciable signal was present. The map was cleaned of the contribution from the side lobes of the array due to incomplete filling of the UV-plane and residual calibration errors. The observations of the calibrator and maser were alternated frequently enough (every 60 s) and the calibrator was sufficiently close to the maser, the amplitudes and phases obtained with the calibrator changed in the transition from the calibrator to the maser insignificantly.

3. RESULTS

3.1. Absolute Positions

Table 1 lists the absolute positions of the strongest spectral features measured by the method described in the previous section.

The positions of the nearest bright infrared sources are also listed. The difference of their positions from those of the masers is of the order of $10''$, and it is comparable to the total extent of the masers. This suggests the association of the methanol masers with young stellar objects, which are these infrared sources.

3.2. Maps

1. OMC-2

The maps of the sources of maser emission obtained with an angular resolution of the order of $0.1''$ represent a set of bright spots, and each spot has, as a rule, its own radial velocity. Table 2 lists the characteristics of individual maser spots.

The 44-GHz map of OMC-2 is given in Fig. 1. It shows three groups of spots arranged along an arc about $5''$ long and curved toward the infrared source IRS 4S. There is also the source of far-infrared radiation at a wavelength of 1300 μm FIR 3 [9], which coincides, within the error limits and with allowance made for the source extent ($24'' \times 12''$), with the methanol maser. The maser is located between the red and blue wings of a bipolar outflow [10, Fig. 2] (see also [11]). The radial velocity of the maser components varies along the arc from 10.75 to 11.9 km s^{-1}. The 95-GHz map of the maser OMC-2 is similar to its 44-GHz map with the same curvature of the maser spots' arrangement toward the infrared source IRS 4S. In the determination of the

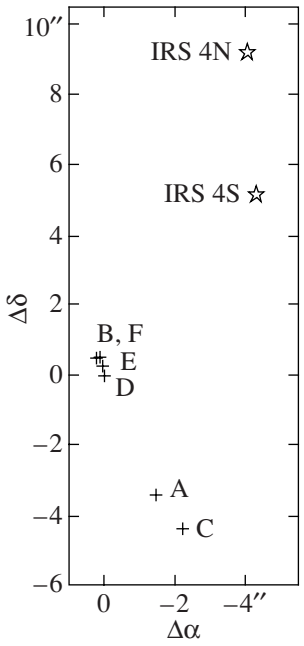

Fig. 1. Map of the methanol maser OMC-2 in the $7_0-6_1A^+$ line at 44-GHz. Asterisks: infrared sources IRS 4N and IRS 4S.

relative positions of the masers and infrared source it was accepted that the coordinates of the brightest features at 95 and 44 GHz coincide. Positions of the remaining maser spots at the two frequencies differ by no more than 0.2″, which is less than the beamwidth at 95 GHz. Thus, we may assume a full conformity of the maser maps at the two frequencies. The fluxes of the strongest maser components are also nearly identical, about 200 Jy. The angular size of the brightest maser spot at 44 GHz is 0.23″ × 0.027″ (92 × 11 AU) with a position angle of the major axis of the fitted ellipse of 79°. Other maser spots have similar sizes. At 95 GHz the maser spots are not resolved by the BIMA beam: the upper limit on the angular size is 0.2″.

2. NGC 2264

Table 3 lists the parameters of the 44 GHz maser spots in NGC 2264.

The map of NGC 2264 in the 44-GHz methanol line is presented in Fig. 2. As in the case of OMC-2, the maser spots are arranged along an arc that is slightly longer than 5″. The arc is bent toward Allen's infrared source IRS 1. The arc length is of the same order of magnitude as the distance from the brightest spot to IRS 1. The radial velocities of the maser spots are 7.22-7.72 km s^{-1} and increase northward. The 95-GHz map of the methanol maser NGC 2264 is similar to the 44-GHz map; it also demonstrates the

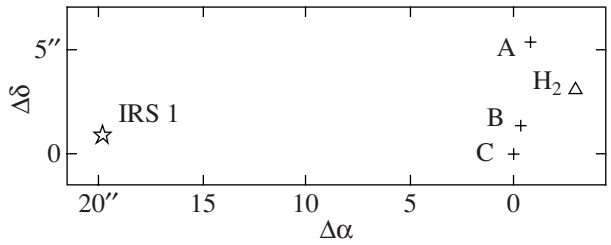

Fig. 2. Map of the methanol maser NGC 2264 in the $7_0-6_1A^+$ line at 44-GHz. Asterisk: infrared source IRS 1; triangle: molecular hydrogen spot Knot A [12].

maser spots arranged along an arc bent toward IRS 1. Their positions coincide, within the error limits, with those of the 44-GHz maser spots. The fluxes of the brightest spots are nearly identical at both frequencies, they are approximately 300 Jy. The angular size of the brightest spot at the radial velocity 7.22 km s^{-1} is 0.07″ × 0.05″ (49 × 35 AU) with a major-axis position angle of 45°. The smaller angular sizes of the spots in NGC 2264 compared to those in OMC-2 are partly due to the greater distance: 700 pc against 400 pc. The methanol maser is at the edge of the molecular cloud centered on IRS 1, near the edge of a bipolar outflow (Fig. 3).

4. EXCITATION OF CLASS I METHANOL MASERS

The universally accepted model of Class I methanol masers assumes that the rotational levels of the methanol molecule are excited by collisions with hydrogen molecules at a sufficiently high kinetic temperature. The maser emission arises due to a specific arrangement of the levels of the methanol molecule, which belongs to the type of a slightly asymmetric top. In the application to Class I masers this property was noted for the first time by Zuckerman et al. [14].

Figure 4 shows for A-methanol the diagram of the levels with rotational quantum number J for two values of the projection of the angular momentum onto the molecule axis K. Other methanol levels affect the excitation of the maser levels weakly. The maser transitions arise between levels belonging to different

Table 3. Characteristics of maser spots in NGC 2264 at 44 GHz

Spot	$\Delta\alpha$	$\Delta\delta$	V_{LSR}, km s^{-1}	Flux density, Jy
A	−0.84″	5.32″	7.72	3.8
B	−0.35	1.39	7.59	83
C	0	0	7.22	330

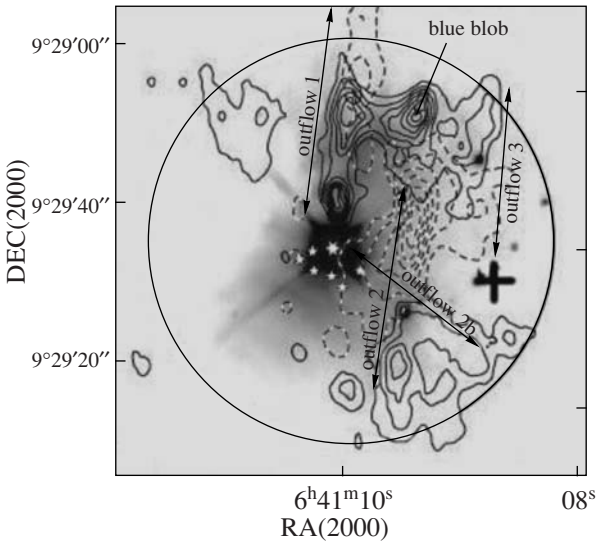

Fig. 3. Maser in the source NGC 2264 (cross) superimposed on the image in the K band (half-tones) and in the CS 2–1 line (solid and dashed contours) from Schreyer et al. [13]. Arrows: bipolar outflows. Allen's source IRS 1 is at the center.

ladders with $K = 0$ and with $K = 1$. The probability of spontaneous transition from levels of the $K = 0$ ladder to the $K = 1$ ladder ($\Delta K = -1$) is much lower than the probability of other allowed spontaneous transitions $\Delta K = 1$ and $\Delta K = 0$ because of the small difference in the energy of the levels and, accordingly, low frequency of emission ν, because the probability of spontaneous emission is proportional to ν^3. In contrast to this, transitions in the opposite direction, with $\Delta K = 1$, have greater probabilities of spontaneous emission, because the frequencies of these transitions are high and lie in the submillimeter wavelength range. The probabilities of submillimeter transitions exceed by 2–3 orders of magnitude the probabilities of spontaneous transitions between signal levels, i.e., between levels corresponding to Class I maser emission. As to spontaneous transitions within the ladders, their probabilities are nearly identical for both ladders and are by an order of magnitude lower than the probabilities of submillimeter-range spontaneous transitions between the ladders. This property of the methanol molecule allows us to make a simple analytical estimate of maser emission intensity.

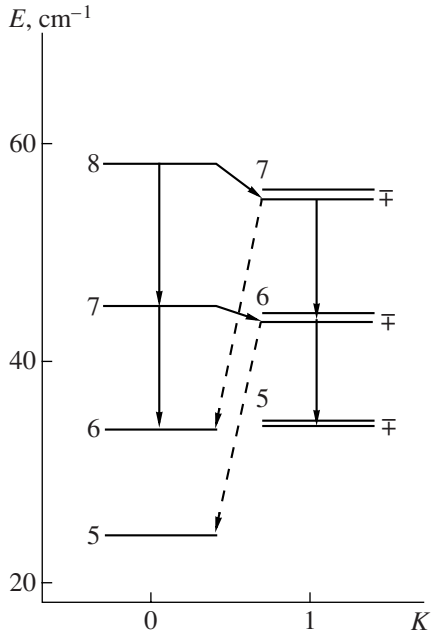

Fig. 4. Level diagram of A-methanol. Oblique arrows from left to right: transitions $7_0-6_1A^+$ and $8_0-7_1A^+$, from right to left: $6_1-5_0A^+$ and $7_1-6_0A^+$, which provide the sink from the lower levels of the maser transitions. Vertical arrows: $7_0-6_0A^+$ and $8_0-7_0A^+$ transitions, which control the populations of the upper levels of the maser transitions, and $6_1-5_1A^+$ and $7_1-6_1A^+$ transitions, which control the populations of the lower levels.

As is well known, the maser emission arises in the presence of inversion of the populations of signal levels, at which the population of the upper level is greater than that of the lower level. The process producing the inversion of the populations of signal levels is called pumping. In Class I methanol masers collisions populate all rotational levels up to the level with the energy that corresponds to the kinetic temperature of the gas. If the rate of collisional transitions is higher than that of all spontaneous radiative transitions, then in the absence of an external radiation field a Boltzmann distribution of populations is established. However, the rich rotational spectrum of methanol includes transitions with very low probabilities of spontaneous emission as well as transitions with a probability of spontaneous transition that is

much higher than the rate of collisional transitions in a certain range of densities and temperatures. For such transitions the population of the upper level is less than the mean population of the nearest levels. As a result, the transition for which this level is the lower one is inverted. Thus, in this case inversion of the transition is provided, instead of the increase in the population of the upper level, by the depopulation of the lower layer through fast spontaneous decay ("sink").

On the diagram of rotational levels of A-methanol (Fig. 4) the lower levels of maser signal transitions are the $J = 6$ and 7, $K = 1$ levels, and the sink from them is provided mainly by spontaneous transitions with $\Delta K = 1$, which have a higher probability. Note that the $K = 0$ ladder includes no levels that can be strongly depopulated by spontaneous transitions. Instead, there are transitions with $\Delta K = -1$ with a small energy difference and a low probability of spontaneous emission. They are the so-called transitions between the signal levels responsible for the maser emission. These problems were discussed in more detail by Kalenskii [15], who calculated the brightness temperature of the emission of Class I methanol masers in some models. In this paper we present the results of a simple calculation of the brightness temperature of the maser emission using only these peculiarities of the methanol rotational spectrum and not requiring the knowledge of particular values of physical parameters such as the methanol column density and temperature, source size, and methanol abundance.

Let us consider the main chain of transitions including maser transitions. The maser emission takes place in the transitions from the upper signal level J_0 to the lower signal level $(J-1)_1$ with the emission at frequencies 44 GHz for $J_0 = 7_0$, 95 GHz for $J_0 = 8_0$, 146 GHz for $J_0 = 9_0$, and so on. The lower signal level $(J-1)_1$ is rapidly depopulated by spontaneous emission in the transition to the level $(J-2)_0$ and, to a lesser degree, in the transition to the level $(J-2)_1$. The last transition will not be taken into account in our approximate estimates, because its probability is an order of magnitude lower, and, in addition, its contribution is mostly compensated for by the spontaneous transition from the upper signal level J_0 to the level within the same ladder $(J-1)_0$. The collisional transitions populate almost all rotational levels equally in the limits determined by the gas temperature and density. In particular, they compensate the decrease in the population of the upper signal level through emission, i.e., they are the source of maser pumping. Because of the low probability of spontaneous emission between signal levels the population of the upper level will remain enhanced relative to that of the lower signal level.

In the cyclic chain of $J_0 \to (J-1)_{-1} \to (J-2)_0 \to J_0$ transitions considered, the last step is provided by collisions, which can have a sufficient rate at an appropriate temperature and density of the gas. The first step of the chain is a bottleneck, and it sets a low value of the circulation rate throughout the chain at spontaneous emission between signal levels. However, the circulation rate can become much higher when the stimulated emission is added to the spontaneous one: the role of the stimulated emission increases with maser radiation density. Since the signal levels are always inverted, in stimulated transitions, the radiative transitions prevail over the absorptive ones. With increasing radiation density the rate of stimulated transitions grows exponentially: this is the maser effect.

The increase in the rate of stimulated transitions will continue until the rate of transitions to the lower signal level becomes equal to the rate of decay (sink) of the lower signal level through the rapid spontaneous emission to the level $(J-2)_0$. In the limit one sink photon is per each maser photon; this restricts the maximum density of Class I maser emission. It can be estimated by equating these two rates:

$$B_1\rho + A_1 = A_2, \tag{1}$$

where the left-hand side is the rate of radiative transitions between the signal levels, including stimulated as well as spontaneous transitions. Quantities B_1 and A_1 are the Einstein coefficients for the signal transitions. The right-hand side (A_2) is the Einstein coefficient of spontaneous transitions depopulating the lower signal level.

The radiation density is

$$\rho = \frac{\Omega}{4\pi}\frac{8\pi k T_B \nu^2}{c^3}, \tag{2}$$

where Ω is the solid angle of maser emission, T_B is the brightness temperature, and ν is the frequency. Using the relation between the Einstein coefficients A and B

$$B = \frac{c^3}{8\pi h\nu^3}A \tag{3}$$

and neglecting the contribution of spontaneous maser emission, we obtain a simple formula,

$$\frac{\Omega}{4\pi}\frac{kT_B}{h\nu}A_1 = A_2 \tag{4}$$

(k and h are the Boltzmann and Planck constants, respectively). Hence, we find the brightness temperature:

$$T_B = \frac{4\pi}{\Omega}\frac{h\nu}{k}\frac{A_2}{A_1} \tag{5}$$

from here is received.

For the isotropic case, we have $\Omega = 4\pi$, and the brightness temperature is determined solely by

Table 4. Limiting brightness temperatures of isotropic Class I maser emission of A-methanol and E-methanol

A-methanol				E-methanol			
J	ν, GHz	A_2/A_1	T_B, K	J	ν, GHz	A_2/A_1	T_B, K
7	44.1	3137	6635	4	36.2	302	522
8	95.2	376	1716	5	84.5	44	177
9	146.6	123	863	6	132.9	18.5	118
10	198.4	59	562	7	181.3	10.9	95
11	250.5	35	421	8	229.8	7.6	84
12	302.9	22.5	327				
13	355.6	16.1	274				
14	408.6	12.2	239				

methanol molecular characteristics: the probability of spontaneous emission from the upper and lower signal levels and the maser emission frequency. This is the limiting brightness temperature, and it does not depend on the physical conditions in the maser source *within the limits of the boundary conditions of temperature and density as well as the methanol abundance and linear sizes*. As a rule, in actual maser sources these conditions are satisfied. In the case of directional emission within solid angle Ω the brightness temperature will be higher by a factor of $4\pi/\Omega$.

Using formula (5) we calculated the limiting brightness temperatures of isotropic maser emission for various A-methanol transitions. Table 4 lists the results of our calculations. The table gives also the values of the brightness temperature for Class I maser $J_{-1} \to (J-1)_0$ transitions for E-methanol, which has a similar structure of the levels.

The characteristics of maser emission, such as intensity (brightness temperature) and line narrowing, depend on the extent to which the stimulated emission exceeds the spontaneous emission between the signal levels, i.e., on the ratio A_2/A_1 (since $A_2 \sim B\rho$). As we see from Table 4, the most prominent maser transition with the greatest ratio A_2/A_1 is the $7_0{-}6_1A^+$ transition at 44 GHz, in accordance with the results of observations. The masers next in strength are the maser in the transition $8_0{-}7_1A^+$ at 95 GHz and the somewhat weaker maser in the transition $4_{-1}{-}3_0E$. With increasing J the ratio A_2/A_1 decreases and becomes of the order of 10, which is already not sufficient for the appearance of a strong maser emission at $J = 14$ in A-methanol and at $J = 7$ in E-methanol. Furthermore, with increasing J the energy of the levels increases and the population accordingly decreases; this was not taken into account when compiling Table 4. As a result, the maser emission lines at higher J should be broader and less intense, which is consistent with the observations.

From the A-methanol transitions listed in Table 4 (at the left) maser emission has been observed at the frequencies 44.1, 95.2, and 146.6 GHz. In E-methanol maser emission has been found in transitions at the frequencies 36.2, 84.5, 132.9, and 229.8 GHz. The data of the table demonstrate that the maser emission of A-methanol should be observed as well at higher frequencies, from 198.4 to 408.6 GHz. In E-methanol masers at 181.3 GHz are predicted. The expected intensity at these frequencies is lower than that at lower frequencies. Nevertheless, the detection of maser emission in E-methanol at frequency 229.8 GHz in the sources DR 21(OH) and DR 21W [16] suggest the possibility of the existence, at least in these sources, of maser emission in other high-frequency transitions, especially in A-methanol.

A peculiarity of the methanol masers is a considerable, by almost an order of magnitude, excess of A-methanol masers above E-methanol masers, which is also observed. The maser emission at $J < 7$ for A-methanol and at $J < 4$ for E-methanol is replaced by anomalous absorption, because the upper and lower signal levels change their places, and the transition inversion becomes its opposite—antiinversion. However, in the presence of strong infrared emission transitions with $J < 7$ in A-methanol and with $J < 4$ in E-methanol can become inverted and produce Class II maser emission. For instance, in the $5_1{-}6_0A^+$ transition the strong Class II maser emission at 6.7 GHz is observed. In this paper, Class II masers are not considered.

5. EMISSION DIRECTIVITY

In the VLA observations of methanol masers at 44 GHz, we managed to map the distribution of maser spots as well as to resolve the maser spots themselves. Therefore, it has become possible to estimate their brightness temperature. For the brightest spot in OMC-2, the brightness temperatures is $T_B = 1.74 \times 10^7$ K and $T_B = 3.9 \times 10^7$ K in NGC 2264. According to Table 2, the theoretical brightness temperature is $T_B = (4\pi/\Omega) \times 6635$ K. Comparing the calculated brightness temperature with the measured one, we find the maser directivity $4\pi/\Omega = 5.9 \times 10^3$ for NGC 2264 and $4\pi/\Omega = 2.6 \times 10^3$ for OMC-2. The corresponding values of the emission opening angle are 3° for NGC 2264 and 4.5° for OMC-2. Using the measured linear sizes of the maser spots, we can estimate the depth of the masing region from the opening angle, $L \sim 1000$ AU for both masers.

6. MODEL OF CLASS I MASERS

When estimating the radiation density inside the source, we assume that the spontaneous emission of the sink from the lower signal level freely escapes from the source experiencing no absorption and subsequent stimulated emission, i.e., that the optical depth for a given line is less than unity. In the case of a large optical depth in the maser line necessary for the maser action, the optical depth in the transition providing the sink is also large. In this case, the sink emission is trapped within the source; this emission is absorbed, increasing the population of the upper level of the sink transition, which is the lower signal level. Thus, the depopulating effect of spontaneous emission from the lower signal level will be balanced. At the same time, the optical depth in the direction of propagation at the maser emission frequency should be fairly large. In the isotropic case of large optical depth in all the involved lines, maser emission does not arise. The anisotropy of high-directivity maser emission together with the isotropic spontaneous emission of the sink allows us to resolve this contradiction in certain geometric models of the source. If the emission source has the shape of a thin cylinder, then high-gain maser emission propagates along its axis and photons of the sink whose spontaneous emission isotropic freely escape from the cylinder across its axis. According to the estimates of Section 5, in this model the ratio of the cylinder length to its diameter in the methanol masers OMC-2 and NGC 2264 is of the order of 30. Thus, under certain conditions strong maser emission can be provided, because the optical depth across the cylinder for sink photons is smaller than that along the cylinder by a factor of 30.

The cylindrical geometry of an elongated source can be realized in other models, e.g., in the model of a thin spherical or oval envelope and even in the model of a homogeneous cloud. Inside the cloud there is a core, in which at a large optical depth, the populations of the levels are thermalized by their own emission. However, in a thin layer near to the cloud surface, the sink emission escapes to the hemisphere that is external relative to the core, and the maser lines remain inverted. This model was discussed by Kalenskii [15]. The emission in a maser line has the greatest intensity in the direction tangential to the surface (Fig. 5a). In an ideal case, the observer should see a ring-shaped source. In actual sources, the envelope can be highly inhomogeneous; therefore, the ring breaks up into separate maser spots. However, their distribution reflects the ring-like shape of the source.

Figure 5b shows one of the versions of this model. The optical depth of the cloud in maser lines is insignificant, and masers do not arise anywhere at its boundary. However, near the cloud boundary there is a region with an enhanced column density of methanol. The column density can be enhanced due to a local increase in the methanol density and (or) abundance, e.g., under the action of a shock wave. In this case, masers can appear only in a small segment of the cloud boundary.

Precisely this distribution of maser spots was found in OMC-2 and NGC 2264. The maser spots are arranged along arcs; near the arc centers of curvature, there are the activity centers IRS 4S in OMC-2 and Allen's object IRS 1 in NGC 2264.

Figure 5c presents a version of Kalenskii's model in which the sink of photons is realized through the cavity formed by a high-velocity jet. The regions where masers can appear are located at the cavity boundary (crosses in the figure).

7. DISCUSSION

The infrared source IRS 4S in OMC-2 drives the bipolar outflow observed in the CO line [17], which, interacting with the surrounding interstellar gas, produces a shock wave exciting molecular hydrogen emission [5]. According to the hypothesis of Plambeck and Menten [2], the same shock wave excites Class I methanol maser emission. Our new high-resolution maps have enabled us to compare the positions of the maser spots and clumps of excited molecular hydrogen. In the region where the maser spots of interest to us are located, there are clumps of molecular hydrogen with numbers 67–73 from the catalog of Yu et al. [18]. None of the maser spots coincides with a clump; thus, we have found no confirmation for the hypothesis of Plambeck and Menten.[1] The infrared source IRS 4 is a pair of protostars with luminosity $L = 10^3 L_\odot$ [19]. It is surrounded by a molecular core, which is traced also in submillimeter emission of dust (the sources FIR 3 [9, 11] and CSO 22 [20]). The methanol masers spots are localized at the outskirts of the core in a segment

[1] The vibrational lines of molecular hydrogen arise in hot regions with a temperature of the order of or above 1000 K, whereas at such a temperature either methanol molecules can dissociate or high-lying methanol levels are populated and the population of the fairly low-lying signal levels of the $7_0-6_1A^+$ line (Fig. 4) is insufficient for a strong methanol emission at 44 GHz. Within the framework of the hypothesis of Plambeck and Menten, we must admit that the masers arise either in the already cooled gas or in the regions where the shock velocity is low and the postshock temperature increase does not exceed ~200 K. This is sufficient for the evaporation of dust grain mantles, but not sufficient for the excitation of H_2 emission. Therefore, the noncoincidence between the positions of masers and H_2 emission sources cannot serve as a ground for rejecting the hypothesis of Plambeck and Menten. The role of bipolar outflows will be considered in our forthcoming works; in this paper, we consider an alternative model.

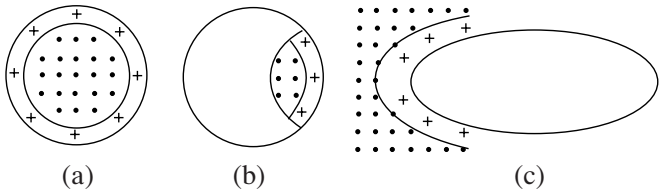

Fig. 5. Models of Class I methanol masers: (a) the model proposed by Kalenskii [15], (b) its version in which the region with an enhanced methanol column density occupies a small part of the cloud adjacent to its boundary, (c) version of the model in which the sink of photons is realized through the cavity formed by a high-velocity jet. The crosses indicate the sites at which the observer placed at a perpendicular to the figure plane can see masers; the dots indicate the regions where the gas is thermalized.

of an arc surrounding IRS 4 on one side and are associated with the bipolar outflow [10, 11].

In NGC 2264, the activity center is Allen's source IRS 1 located in the core of a dense molecular cloud [21] framed from one side by methanol maser spots. According to the measurements of Schreyer et al. [21], at the cloud center the gas density is $n = 2 \times 10^6$ cm^{-3} and the kinetic temperature is 55 K. The methanol abundance in the cloud is 9×10^{-9}, and its extent is about 2.5×10^{16} cm, or 1500 AU. The extent of the arc on which the methanol maser spots are arranged is of the same order of magnitude. The spots do not coincide positionally with an infrared source or any other object. As in the case of OMC-2, such a geometry is consistent with the model of an inverted thin spherical envelope surrounding a thermalized dense molecular core. The maser emission propagates tangentially to the envelope in the direction of the greatest optical depth. The observed brightness temperature, of the order of 10^7 K, is consistent with the brightness temperature that is obtained in models "c" and "d" of Kalenskii [15] with the following parameters: $n = 3 \times 10^6$ cm^{-3}, methanol abundance 10^{-7}, and kinetic temperature 30 K. The methanol abundance adopted in the model is an order of magnitude greater than that measured in the dense core. Probably, in the outer envelope the methanol abundance is enhanced due to the evaporation of dust particles, which contain methanol ice, along with water. Furthermore, the kinetic temperature 30 K is lower that the measured 55 K; this explains the relative weakness of the 95-GHz methanol maser emission in the model compared to the observed one.

The absence of any physical objects toward individual maser spots most likely implies that the maser emission originates in the entire volume of gas, at least in the envelope. As indicated by Kalenski [15], the observed fragmentation of the masing ring can be due to a sufficiently strong inhomogeneity of the envelope. Indirect evidence that the maser emission arises in a gas volume rather than in physically isolated clumps of material is the presence (found in many sources) of inversion of methanol maser transitions throughout the molecular cloud, as measured from the intensity ratio of the corresponding thermal methanol lines [22]. The inversion is due to the properties of the rotational levels of the methanol molecule considered in Section 2. Thus, the entire molecular cloud can be a source of weak emission in transitions with inverted levels, which, at a small optical depth, should not demonstrate maser characteristics. Only at the sites of the cloud envelope where the methanol abundance is enhanced and (or) there are directions with a large optical depth and small velocity gradient will a bright maser spot be observed.

8. CONCLUSIONS

In OMC-2 and NGC 2264, the methanol maser spots are distributed along arcs bent toward infrared sources that are young stellar objects. The length of these lines is approximately equal to the distance to the infrared sources, which lie near the centers of curvature of the lines were the spots are located. The distributions of the maser spots at two frequencies, in the 44 and 95 GHz methanol lines, are virtually identical, and the fluxes from the brightest spots are similar. The measured sizes of the maser spots are, on average, about 50 AU. At 95 GHz, where the synthesized beamwidth is larger than at 44 GHz, the maser spots are not resolved with an upper limit on the linear size of 100 AU. The brightness temperature of the strongest components in the 44 GHz line is 1.7×10^7 and 3.9×10^7 K for OMC-2 and NGC 2264, respectively. In the simplified model of a Class I maser, the limiting maser radiation density does not depend on the temperature, density, methanol abundance, or source size and is determined solely by the ratio of the probability of the sink spontaneous emission to the probability of spontaneous emission between the signal levels of the maser transition. In the isotropic case, the estimated brightness temperature at 44 GHz is several orders of magnitude lower than the measured brightness temperature. Hence, we estimated the maser emission directivity corresponding

to opening angles of 3° and 4.5° for NGC 2264 and OMC-2, respectively. The depth of the emitting region is about 1000 AU. The emission directivity is naturally realized in the model of a maser consisting of a dense, nonradiating core and a thin envelope, probably with an enhanced methanol abundance. The maser emission has the greatest intensity in the direction tangential to the envelope. The expected pattern of a ring-shaped or elliptical intensity distribution is disrupted by a deviation of the envelope from symmetry and inhomogeneity in the distribution of the gas density, temperature, and methanol abundance. The size of the radiating envelope estimated from the measured depth and extent of the spot is 2×10^4 AU, or 0.15 pc. This size is close to the sizes of the dense molecular cores surrounding the young stellar objects IRS 4 in OMC-2 and IRS 1 in NGC 2264.

ACKNOWLEDGMENTS

This work was supported by the Russian Foundation for Basic Research (project no. 07-02-00248).

REFERENCES

1. K. M. Menten, in *Proc. of the 3rd Haystack Observatory Meeting Skylines*, Ed. by A. D. Haschick and P. T. P. Ho, ASP Conf. Ser. **16**, 119 (1991).
2. R. L. Plambeck and K. M. Menten, Astrophys. J. **364**, 555 (1990).
3. S. Liechti and C. M. Walmsley, Astron. Astrophys. **321**, 625 (1997).
4. A. M. Sobolev, W. D. Watson, and V. A. Okorokov, Astrophys. J. **590**, 333 (2003).
5. Y. Pendleton, M. W. Werner, R. Capps, and D. Lester, Astrophys. J. **311**, 360 (1986).
6. D. A. Allen, Astrophys. J. Lett. **172**, L55 (1972).
7. S. Kurtz, P. Hofner, and C. V. Alvarez, Astrophys. J. Suppl. Ser. **155**, 149 (2004).
8. V. I. Slysh, I. E. Val'tts, S. V. Kalenskiĭ, and V. V. Golubev, Astron. Zh. **76**, 892 (1999) [Astron. Rep. **43**, 785 (1999)].
9. R. Chini, Bo Reipurth, D. Ward-Thompson, et al., Astrophys. J. Lett. **474**, L135 (1997).
10. J. P. Williams, R. L. Plambeck, and M. H. Heyer, Astrophys. J. **591**, 1025 (2003).
11. Y. Shimajiri, S. Takahashi, S. Takakuwa, et al., Astrophys. J. **683**, 255 (2008).
12. H. Wang, J. Yang, M. Wang, and J. Yan, Astron. Astrophys. **389**, 1015 (2002).
13. K. Schreyer, B. Stecklum, H. Linz, and Th. Henning, Astrophys. J. **599**, 335 (2003).
14. B. E. Zuckerman, B. E. Turner, D. R. Johnson, et al., Astrophys. J. **177**, 601 (1972).
15. S. V. Kalenskiĭ, Astron. Zh. **72**, 524 (1995) [Astron. Rep. **39**, 465 (1995)].
16. V. I. Slysh, S. V. Kalenskiĭ, and I. E. Val'ts, Astron. Zh. **79** (2002) [Astron. Rep. **46**, 216 (2002)].
17. J. Fischer, D. B. Sanders, M. Simon, and P. M. Solomon, Astrophys. J. **293**, 508 (1985).
18. K. C. Yu, J. Bally, and D. Devine, Astrophys. J. Lett. **485**, L45 (1997).
19. J. J. Johnson, R. D. Gehrz, R. D. Jones, et al., Astron. J. **100**, 518 (1990).
20. D. C. Lis, E. Serabyn, J. Keene, et al., Astrophys. J. **509**, 299 (1998).
21. K. Schreyer, F. P. Helmich, E. F. van Dishoeck, and Th. Henning, Astron. Astrophys. **326**, 347 (1997).
22. V. I. Slysh, S. V. Kalensky, I. E. Val'tts, et al., Astrophys. J. Suppl. Ser. **123**, 515 (1999).

Translated by G. Rudnitskii